



# Multifunctional indanone–chalcone hybrid compounds with anti- $\beta$ -amyloid ( $A\beta$ ) aggregation, monoamine oxidase B (MAO-B) inhibition and neuroprotective properties against Alzheimer's disease

Keren Wang<sup>1</sup> · Lintao Yu<sup>1</sup> · Jian Shi<sup>1</sup> · Wenmin Liu<sup>1</sup> · Zhipei Sang<sup>1</sup>

Received: 11 April 2019 / Accepted: 12 August 2019  
© Springer Science+Business Media, LLC, part of Springer Nature 2019

## Abstract

To discover multifunctional agents for the treatment of Alzheimer's disease (AD), a series of indanone–chalcone hybrid compounds were designed and synthesized based on the multitarget-directed ligand strategy. Their monoamino oxidases (MAO-A and MAO-B) and  $A\beta_{1-42}$  aggregation inhibitory activities were evaluated. The results were shown that all synthetic compounds exhibited mostly good multifunctional activities. Among all, compound **TM-11** represented the best  $A\beta_{1-42}$  aggregation inhibitory potency ( $IC_{50} \sim 1.8 \mu M$ ) and good disaggregation activity ( $IC_{50} \sim 7.9 \mu M$ ). Both TEM images and docking studies provided good reasonable explanation to the hypothesis. Meanwhile, compound **TM-11** was a selective MAO-B inhibitor, as well as a neuroprotective agent against  $A\beta_{1-42}$ -induced toxicity. Based on the structural considerations, the lipophilicity of the compound **TM-11** could render to pass through blood–brain barrier (BBB) in vitro in accordance with the Lipinski's rule of five. In conclusion, these results were suggested that compound **TM-11** might be a potential multifunctional agent for the treatment of AD.

**Keywords** Alzheimer's disease · Indanone–chalcone hybrid molecules · MAO-B inhibition ·  $A\beta_{1-42}$  aggregation inhibition · Neuroprotective effects

## Abbreviations

AD	Alzheimer's disease
AChEIs	acetylcholinesterase inhibitors
ACh	acetylcholine
$A\beta$	$\beta$ -amyloid
MAO-B	monoamine oxidase B
MAO-A	monoamine oxidase A
MTDLs	multitarget-directed ligands
ThT	thioflavin T
TEM	transmission electron microscopy
PDB	protein data bank

MTT	3-(4,5-dimethylthiazol-2-yl)-2,5-diphenyltetrazolium
PAMPA-	parallel artificial membrane assay for the
BBB	blood–brain barrier
TPSA	topological polar surface area
ADME	absorption, distribution, metabolism, excretion.

## Introduction

Alzheimer's disease (AD) is an age-related incurable neurodegenerative disease characterized by deterioration of memory, language skills, and other cognitive impairments. It is reported that the total estimated worldwide cost of dementia is US\$818 billion in 2015, this number will increase to 2 trillion dollar by 2030, and its prevalence will increase to 131 million by 2050 (Alzheimer's Disease International 2015). The current drugs mainly focused on acetylcholinesterase inhibitors (AChEIs), such as donepezil, rivastigmine, and galantamine. The clinical use shows that these drugs aim to the treatment of symptoms, but they do not halt or reverse the progress of this disease (Ferreira-Vieira et al. 2016).

These authors contributed equally: Keren Wang, Lintao Yu

**Supplementary information** The online version of this article (<https://doi.org/10.1007/s00044-019-02423-4>) contains supplementary material, which is available to authorized users.

✉ Zhipei Sang  
sangzhipei@126.com

<sup>1</sup> College of Chemistry and Pharmaceutical Engineering, Nanyang Normal University, Nanyang 473061, China

Although the pathogenesis of AD is not clear, the main pathological features, such as low levels of acetylcholine (ACh), deposits of amyloid- $\beta$  ( $A\beta$ ) and  $\tau$  protein have been considered to be an important factor in the pathogenesis of AD (Lane et al. 2018). Particularly, accumulation of amyloid-beta ( $A\beta$ ) in the brain is a central event in the pathogenesis of AD based on the “amyloid hypothesis”,  $A\beta$  could initiate the pathogenic cascade, generates reactive oxygen species and tau phosphorylation, which ultimately lead to neuronal loss and dementia (Ricciarelli and Fedele 2017; Sensi et al. 2018). Therefore, inhibiting  $A\beta_{1-42}$  aggregation would provide a potent therapeutic strategy for AD treatment.

Monoamine oxidase (MAO) is an important FAD-dependent enzyme (flavoenzymes) responsible for the metabolism of neurotransmitters such as dopamine, serotonin, adrenaline, and noradrenaline (Kumar et al. 2017). MAO exists in two types, MAO-A and MAO-B. MAO-B expression significantly increases in the brain of AD patients, and selective MAO-B inhibitor Selegiline could improve learning and memory deficits in animal models associated with AD (Borroni et al. 2017). Thus, selective MAO-B inhibitors seem to be an important treatment of AD.

Due to the complexity of AD, the multitarget-directed ligands (MTDLs), which possess two or more complementary AD-related targets, have been considered as an effective way for the treatment of AD. The obtained results encourage many groups to develop the advanced multi-function agents (Cavalli et al. 2008; de Freitas Silva et al. 2018; Umar and Hoda 2017).

Chalcones ( $\alpha$ -phenyl- $\beta$ -benzoyl ethylene) and their derivatives are important bioactive molecules that have been studied to exhibit impressive biological activities such as

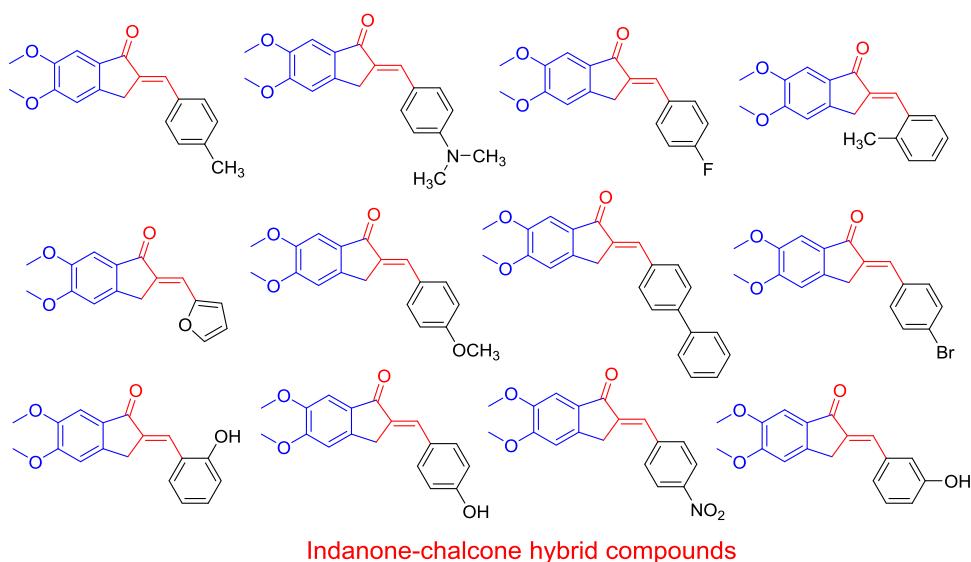
radical-scavenging, antitumor, anti-inflammatory, and neuroprotective properties (Zhuang et al. 2017). Indanone is one of the privileged structures in medicinal chemistry and it is commonly associated with various pharmacologically active compounds (Patil et al. 2017). Indanones and their derivatives have been studied to determine their biological activities within disease states, including AD (Li et al. 2016; Caliandro et al. 2018; Costanzo et al. 2016; Huang et al. 2012). Based on the MTDLs strategy, we report the design, synthesis, and evaluation of a series of indanone–chalcone hybrid compounds (Fig. 1) that are found to indicate potentially applicable biological activities, including the inhibition of self-induced  $A\beta$  aggregation, inhibition of MAO-B activity, and neuroprotective properties.

## Material and methods

### Experimental section

All chemical agents were obtained from commercial suppliers and used without further purification.  $^1\text{H}$  NMR and  $^{13}\text{C}$  NMR spectra were recorded on a Varian INOVA spectrometer, using tetramethyl silane as an internal standard in  $\text{CDCl}_3$  at 400 and 100 MHz, respectively. Coupling constants were given in Hz. Multiplicities were given as s (singlet), d (doublet), dd (double-doublet), t (triplet), q (quadruplet), m (multiplet), and br (broad signal). MS spectra data were obtained on an Agilent-6210 TOF LC-MS spectrometer. High-performance liquid chromatography (HPLC) analysis was carried out on a Waters600-2487 plus system with the use of a Kromasil C-18 column (4.6 mm  $\times$  250 mm, 5  $\mu\text{m}$ ). The purity of target compounds were confirmed more than 97% by HPLC analysis.

**Fig. 1** Design strategy for the indanone–chalcone hybrid compounds



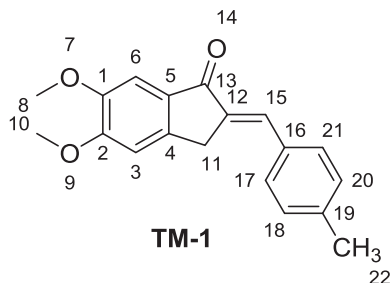
Recombinant human MAO-A and MAO-B (5 mg/mL) were obtained from Sigma–Aldrich. Thioflavin T (ThT) was purchased from TCI (Shanghai) Development. 1,1,1,3,3,3-hexafluoro-2-propanol (HFIP) was purchased from Energy Chemical. Amyloid- $\beta_{1-42}$  ( $A\beta_{1-42}$ ), supplied as trifluoroacetate salt, was purchased from China Peptides Co., Ltd. Docking studies were performed using the AUTODOCK 4.2.6 program.

## Chemistry

### General procedure for the preparation of indanone–chalcone hybrid compounds TM-1–TM-12

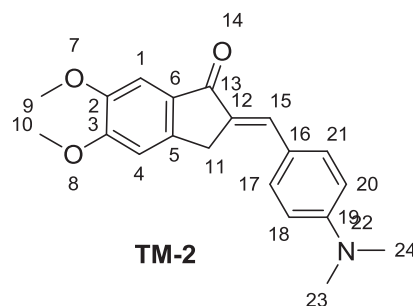
To a mixture of 5,6-dimethoxy-1-indanone (1 mmol) in EtOH (3 mL) was added the appropriate benzaldehyde (1 mmol). An amount of a 30% aqueous KOH (4 mmol) solution was then slowly added dropwise to the reaction. The mixture was stirred for 72 h at 50 °C. After cooling to room temperature, 10% HCl was added dropwise to the mixture making pH = 2, overnight, a yellow precipitate formed and filtrated, the residue was recrystallized with 80% ethanol to give yellow solid **TM-1–TM-12**.

**(Z)-5,6-Dimethoxy-2-(4-methylbenzylidene)-2,3-dihydro-1H-inden-1-one (TM-1)** Light yellow solid, m.p.: 98.6–99.9 °C, 86.7% yield, 98.9% HPLC purity.  $^1\text{H}$  NMR (400 MHz, DMSO- $d_6$ ):  $\delta$  = 7.64 (d,  $J$  = 8.0 Hz, 2H, 2  $\times$  Ar-H), 7.40 (s, 1H, C=CH), 7.31 (d,  $J$  = 8.0 Hz, 2H, 2  $\times$  Ar-H), 7.22 (s, 2H, 2  $\times$  Ar-H), 3.97 (s, 2H, phCH $_2$ ), 3.90 (s, 3H, OCH $_3$ ), 3.84 (s, 3H, OCH $_3$ ), 2.36 (s, 3H, CH $_3$ ).  $^{13}\text{C}$  NMR (100 MHz, DMSO- $d_6$ ), 193.3 (C-13), 155.7 (C-2), 149.8 (C-1), 145.5 (C-5), 139.9 (C-4), 135.4 (C-15), 132.8 (C-19), 131.5 (C-12), 131.0 (C-18, 20), 130.5 (C-16), 130.1 (C-17), 108.5 (C-3), 105.0 (C-6), 56.5, 56.1 (C-8, 10), 32.1 (C-11), 21.5 (C-22). IR (cm $^{-1}$ ): 3100–2900 (–CH $_3$ , –CH), 1683 (C=O), 1363 (–CH $_3$ ), 1253, 1087 (C–O–C). MS (ESI) m/z 295.1 [M + H] $^+$ .

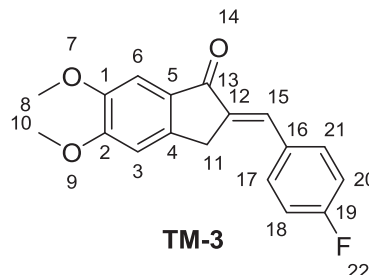


**(Z)-2-(4-(Dimethylamino)benzylidene)-5,6-dimethoxy-2,3-dihydro-1H-inden-1-one (TM-2)** Light yellow oil, m.p.: 117.8–119.1 °C, 83.1% yield, 98.6% HPLC purity.  $^1\text{H}$  NMR

(400 MHz, DMSO- $d_6$ ):  $\delta$  = 7.57 (d,  $J$  = 8.8 Hz, 2H, 2  $\times$  Ar-H), 7.54 (s, 1H, C=CH), 7.34 (s, 1H, Ar-H), 6.96 (s, 1H, Ar-CH), 6.72 (d, 2H,  $J$  = 7.6 Hz, 2  $\times$  Ar-H), 3.99 (s, 3H, OCH $_3$ ), 3.95 (s, 3H, OCH $_3$ ), 3.90 (s, 2H, phCH $_2$ ), 3.04 (s, 6H, 2  $\times$  NCH $_3$ ).  $^{13}\text{C}$  NMR (100 MHz, DMSO- $d_6$ ), 192.3 (C-13), 154.8 (C-3), 151.0 (C-19), 149.4 (C-2), 144.4 (C-6), 133.4 (C-5), 132.5 (C-17, 21), 131.7 (C-15), 130.6 (C-12), 123.4 (C-16), 111.9 (C-18, 20), 107.2 (C-4), 105.0 (C-1), 56.2, 56.1 (C-9, 10), 40.1 (C-23, 24), 32.4 (C-11). IR (cm $^{-1}$ ): 3100–2900 (–CH $_3$ , –CH), 1675 (C=O), 1365 (–CH $_3$ ), 1253, 1002 (C–O–C), 1303 (=N–). MS (ESI) m/z 324.2 [M + H] $^+$ .

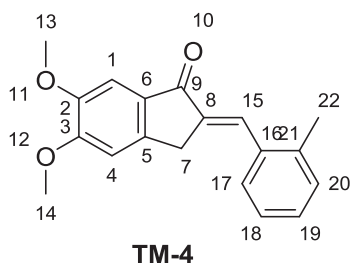


**(Z)-2-(4-Fluorobenzylidene)-5,6-dimethoxy-2,3-dihydro-1H-inden-1-one (TM-3)** Yellow solid, m.p.: 116.9–118.3 °C, 85.8% yield, 98.7% HPLC purity.  $^1\text{H}$  NMR (400 MHz, DMSO- $d_6$ ):  $\delta$  = 7.89 (d,  $J$  = 7.6 Hz, 1H, Ar-H), 7.77 (d,  $J$  = 8.0 Hz, 1H, Ar-H), 7.65 (s, 1H, C=CH), 7.52 (t,  $J$  = 7.6 Hz, 1H, Ar-H), 7.36 (t,  $J$  = 7.6 Hz, 1H, Ar-H), 7.24 (s, 1H, Ar-H), 7.19 (s, 1H, Ar-H), 3.96 (s, 2H, phCH $_2$ ), 3.90 (s, 3H, OCH $_3$ ), 3.85 (s, 3H, OCH $_3$ ).  $^{13}\text{C}$  NMR (100 MHz, DMSO- $d_6$ ), 191.9 (C-13), 156.1 (C-19), 149.9 (C-2), 146.0 (C-1), 138.9 (C-5), 134.9 (C-4), 133.7 (C-15), 131.4 (C-12), 130.9 (C-16), 130.3 (C-17), 129.3 (C-21), 128.6 (C-18), 126.1 (C-20), 108.5 (C-3), 105.2 (C-6), 56.5, 56.2 (C-10), 31.3 (C-11). IR (cm $^{-1}$ ): 3070–2832 (–CH $_3$ , –CH), 1679 (C=O), 1365 (–CH $_3$ ), 1253, 1006 (C–O–C), 1222 (C–F). MS (ESI) m/z 299.1 [M + H] $^+$ .

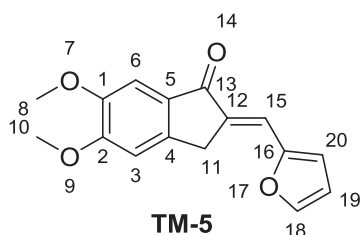


**(Z)-5,6-Dimethoxy-2-(2-methylbenzylidene)-2,3-dihydro-1H-inden-1-one (TM-4)** Light yellow solid, m.p.: 99.6–101.2 °C, 63.6% yield, 99.0% HPLC purity.  $^1\text{H}$  NMR (400 MHz,

DMSO- $d_6$ ):  $\delta$  = 7.70–7.69 (m, 1H, Ar-H), 7.62 (s, 1H, Ar-H), 7.31–7.30 (m, 3H, 3  $\times$  Ar-H), 7.20 (s, 1H, Ar-H), 7.16 (s, 1H, Ar-H), 3.89 (s, 5H, OCH<sub>3</sub> + phCH<sub>2</sub>), 2.41 (s, 3H, CH<sub>3</sub>). <sup>13</sup>C NMR (100 MHz, DMSO- $d_6$ ), 192.1 (C-9), 155.8 (C-3), 149.8 (C-2), 145.8 (C-6), 138.8 (C-5), 137.0 (C-15), 134.2 (C-16), 131.1 (C-21), 130.5 (C-8), 129.6 (C-19), 129.0 (C-20), 128.7 (C-17), 126.7 (C-18), 108.5 (C-4), 105.0 (C-1), 56.4, 56.1 (C-13, 14), 31.6 (C-7), 20.1 (C-22). IR (cm<sup>-1</sup>): 3058–2833 (–CH<sub>3</sub>, –CH), 1683 (C=O), 1357 (–CH<sub>3</sub>), 1255, 1000 (C–O–C). MS (ESI)  $m/z$  295.1 [M + H]<sup>+</sup>.

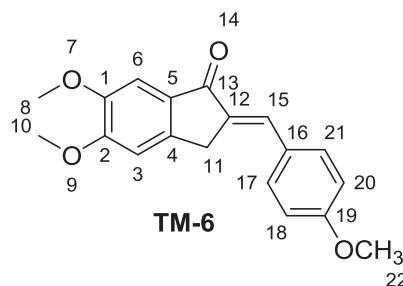


**(Z)-2-(Furan-2-ylmethylene)-5,6-dimethoxy-2,3-dihydro-1H-inden-1-one (TM-5)** Light yellow solid, m.p.: 100.2–101.5 °C, 62.8% yield, 98.1% HPLC purity. <sup>1</sup>H NMR (400 MHz, DMSO- $d_6$ ):  $\delta$  = 7.95 (s, 1H, Ar-H), 7.24 (s, 1H, Ar-H), 7.19 (d,  $J$  = 6.8 Hz, 2H, 2  $\times$  Ar-H), 6.99 (s, 1H, Ar-H), 6.72 (s, 1H, Ar-H), 3.90 (s, 5H, OCH<sub>3</sub> + phCH<sub>2</sub>), 3.83 (s, 3H, OCH<sub>3</sub>). <sup>13</sup>C NMR (100 MHz, DMSO- $d_6$ ), 191.7 (C-13), 155.7 (C-2), 152.0 (C-16), 149.8 (C-1), 146.6 (C-18), 145.2 (C-5), 133.6 (C-4), 130.9 (C-12), 118.2 (C-15), 116.9 (C-3), 113.4 (C-19), 108.6 (C-20), 105.0 (C-6), 56.4, 56.1 (C-8, 10), 32.0 (C-11). IR (cm<sup>-1</sup>): 3100–2834 (–CH<sub>3</sub>, –CH), 1633 (C=O), 1359 (–CH<sub>3</sub>), 1249, 1006 (C–O–C). MS (ESI)  $m/z$  271.1 [M + H]<sup>+</sup>.

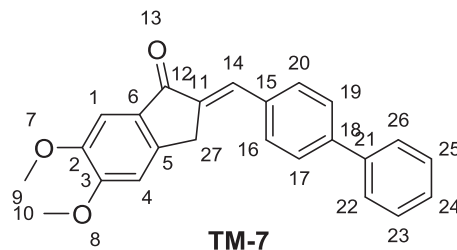


**(Z)-5,6-Dimethoxy-2-(4-methoxybenzylidene)-2,3-dihydro-1H-inden-1-one (TM-6)** Light yellow solid, m.p.: 104.1–105.3 °C, 80.5% yield, 98.6% HPLC purity. <sup>1</sup>H NMR (400 MHz, DMSO- $d_6$ ):  $\delta$  = 7.70 (d,  $J$  = 8.4 Hz, 2H, 2  $\times$  Ar-H), 7.40 (s, 1H, C=CH), 7.21 (s, 2H, 2  $\times$  Ar-H), 7.05 (d,  $J$  = 8.4 Hz, 2H, 2  $\times$  Ar-H), 3.95 (s, 2H, phCH<sub>2</sub>), 3.90 (s, 3H, OCH<sub>3</sub>), 3.83 (s, 6H, 2  $\times$  OCH<sub>3</sub>). <sup>13</sup>C NMR (100 MHz, DMSO- $d_6$ ), 192.3 (C-13), 160.8 (C-19), 155.6 (C-2), 149.8 (C-1), 145.3 (C-5), 133.9 (C-4), 132.8 (C-17,

21), 131.5 (C-12), 130.7 (C-16), 128.2 (C-3), 115.0 (C-18, 20), 108.6 (C-8), 56.4, 56.1 (C-8, 10), 55.8 (C-22), 32.0 (C-11). IR (cm<sup>-1</sup>): 3100–2830 (–CH<sub>3</sub>, –CH), 1687 (C=O), 1361 (–CH<sub>3</sub>), 1259, 1020 (C–O–C). MS (ESI)  $m/z$  311.1 [M + H]<sup>+</sup>.

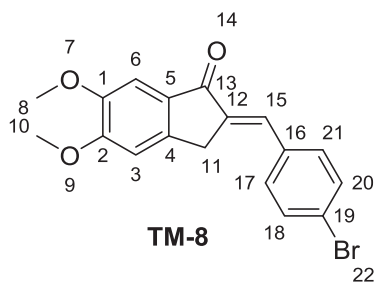


**(Z)-2-([1,1'-Biphenyl]-4-ylmethylene)-5,6-dimethoxy-2,3-dihydro-1H-inden-1-one (TM-7)** Light yellow solid, m.p.: 112.5–113.8 °C, 93.8% yield, 98.9% HPLC purity. <sup>1</sup>H NMR (400 MHz, DMSO- $d_6$ ):  $\delta$  = 7.85 (d,  $J$  = 8.4 Hz, 2H, 2  $\times$  Ar-H), 7.81 (d,  $J$  = 8.4 Hz, 2H, 2  $\times$  Ar-H), 7.76 (d,  $J$  = 8.0 Hz, 2H, 2  $\times$  Ar-H), 7.52–7.48 (m, 3H, 3  $\times$  Ar-H), 7.41 (t,  $J$  = 7.6 Hz, 1H, Ar-H), 7.24 (s, 2H, 2  $\times$  Ar-H), 4.06 (s, 2H, phCH<sub>2</sub>), 3.92 (s, 3H, OCH<sub>3</sub>), 3.85 (s, 3H, OCH<sub>3</sub>). <sup>13</sup>C NMR (100 MHz, DMSO- $d_6$ ), 192.3 (C-12), 155.8 (C-3), 149.9 (C-2), 145.6 (C-6), 141.4 (C-18), 139.7 (C-5), 136.5 (C-21), 134.7 (C-14), 131.6 (C-23, 25), 131.1 (C-15), 130.5 (C-11), 129.5 (C-22, 26), 128.4 (C-24), 127.6 (C-17, 19), 127.2 (C-16, 20), 108.6 (C-4), 105.1 (C-1), 56.5, 56.2 (C-9, 10), 32.2 (C-27). IR (cm<sup>-1</sup>): 3100–2830 (–CH<sub>3</sub>, –CH), 1679 (C=O), 1303 (–CH<sub>3</sub>), 1255, 1004 (C–O–C). MS (ESI)  $m/z$  357.1 [M + H]<sup>+</sup>.

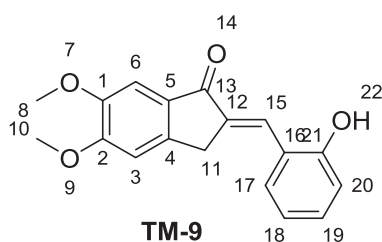


**(Z)-2-(4-Bromobenzylidene)-5,6-dimethoxy-2,3-dihydro-1H-inden-1-one (TM-8)** Light yellow solid, m.p.: 104.6–105.8 °C, 60.8% yield, 98.8% HPLC purity. <sup>1</sup>H NMR (400 MHz, DMSO- $d_6$ ):  $\delta$  = 7.70 (s, 4H, 4  $\times$  Ar-H), 7.40 (s, 1H, Ar-H), 7.22 (d,  $J$  = 6.8 Hz, 2H, 2  $\times$  Ar-H), 3.99 (s, 2H, phCH<sub>2</sub>), 3.91 (s, 3H, OCH<sub>3</sub>), 3.84 (s, 3H, OCH<sub>3</sub>). <sup>13</sup>C NMR (100 MHz, DMSO- $d_6$ ), 192.2 (C-13), 155.9 (C-2), 149.9 (C-1), 145.6 (C-5), 137.2 (C-4), 134.9 (C-15), 132.8 (C-18, 20), 132.4 (C-17, 21), 130.4 (C-16), 130.2 (C-19), 123.4 (C-3), 108.6 (C-6), 56.5 56.2 (C-8, 10),

32.0 (C-11). IR ( $\text{cm}^{-1}$ ): 3100–2800 (–CH<sub>3</sub>, –CH), 1693 (C=O), 1309 (–CH<sub>3</sub>), 1226 (C–Br), 1257, 1004 (C–O–C). MS (ESI)  $m/z$  359.0 [M + H]<sup>+</sup>.

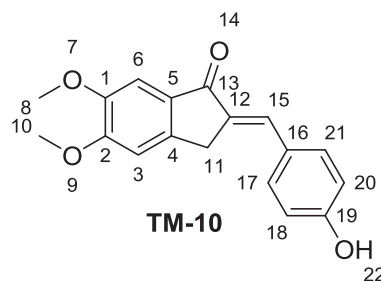


**(Z)-2-(2-Hydroxybenzylidene)-5,6-dimethoxy-2,3-dihydro-1H-inden-1-one (TM-9)** Light yellow solid, m.p.: 137.7–139.2 °C, 53.7% yield, 98.9% HPLC purity. <sup>1</sup>H NMR (400 MHz, DMSO-*d*<sub>6</sub>):  $\delta$  = 10.13 (s, 1H, OH), 7.83 (s, 1H, Ar–H), 7.68 (d, *J* = 7.6 Hz, 1H, Ar–H), 7.27–7.20 (m, 3H, 3 × Ar–H), 6.96–6.89 (m, 2H, 2 × Ar–H), 3.95 (s, 2H, phCH<sub>2</sub>), 3.90 (s, 3H, OCH<sub>3</sub>), 3.84 (s, 3H, OCH<sub>3</sub>). <sup>13</sup>C NMR (100 MHz, DMSO-*d*<sub>6</sub>), 192.4 (C-13), 157.9 (C-21), 155.6 (C-2), 149.8 (C-1), 145.5 (C-5), 134.8 (C-15), 131.4 (C-4), 130.7 (C-12), 129.8 (C-19), 126.3 (C-17), 122.5 (C-18), 119.8 (C-20), 116.4 (C-16), 108.6 (C-3), 105.1 (C-6), 56.4 56.1 (C-8, 10), 32.0 (C-11). IR ( $\text{cm}^{-1}$ ): 3130 (–OH), 3083–2834 (–CH<sub>3</sub>, –CH), 1656 (C=O), 1313 (–CH<sub>3</sub>), 1259, 1010 (C–O–C). MS (ESI)  $m/z$  297.1 [M + H]<sup>+</sup>.

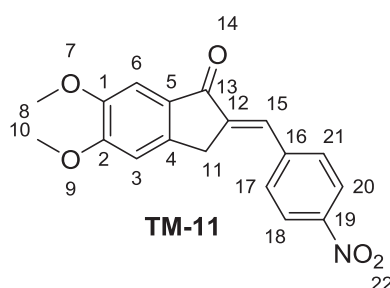


**(Z)-2-(4-Hydroxybenzylidene)-5,6-dimethoxy-2,3-dihydro-1H-inden-1-one (TM-10)** Light yellow solid, m.p.: 140.8–141.9 °C, 46.4% yield, 98.6% HPLC purity. <sup>1</sup>H NMR (400 MHz, DMSO-*d*<sub>6</sub>):  $\delta$  = 10.03 (s, 1H, OH), 7.60 (d, *J* = 8.4 Hz, 2H, 2 × Ar–H), 7.36 (s, 1H, C=CH), 7.20 (d, *J* = 8.4 Hz, 2H, 2 × Ar–H), 6.89 (d, *J* = 8.0 Hz, 2H, 2 × Ar–H), 3.93 (s, 2H, phCH<sub>2</sub>), 3.90 (s, 3H, OCH<sub>3</sub>), 3.83 (s, 3H, OCH<sub>3</sub>). <sup>13</sup>C NMR (100 MHz, DMSO-*d*<sub>6</sub>), 192.4 (C-13), 159.5 (C-19), 155.5 (C-2), 149.7 (C-1), 145.2 (C-5), 133.0 (C-4), 132.9 (C-15), 132.0 (C-12), 130.8 (C-17, 21), 126.7 (C-16), 116.4 (C-18, 20), 108.9, 105.0 (C-6), 56.4 56.1 (C-8, 10), 32.1 (C-11). IR ( $\text{cm}^{-1}$ ): 3210 (–OH), 3000–2800 (–CH<sub>3</sub>, –CH), 1668 (C=O),

1313 (–CH<sub>3</sub>), 1257, 1006 (C–O–C). MS (ESI)  $m/z$  297.1 [M + H]<sup>+</sup>.



**(Z)-5,6-Dimethoxy-2-(4-nitrobenzylidene)-2,3-dihydro-1H-inden-1-one (TM-11)** Light yellow solid, m.p.: 98.9–100.2 °C, 81.3% yield, 98.9% HPLC purity. <sup>1</sup>H NMR (400 MHz, DMSO-*d*<sub>6</sub>):  $\delta$  = 8.30 (d, *J* = 8.4 Hz, 2H, 2 × Ar–H), 7.99 (d, *J* = 8.8 Hz, 2H, 2 × Ar–H), 7.50 (s, 1H, C=CH), 7.23 (s, 2H, 2 × Ar–H), 4.05 (s, 2H, phCH<sub>2</sub>), 3.92 (s, 3H, OCH<sub>3</sub>), 3.84 (s, 3H, OCH<sub>3</sub>). <sup>13</sup>C NMR (100 MHz, DMSO-*d*<sub>6</sub>), 192.0 (C-13), 156.2 (C-2), 149.9 (C-1), 147.6 (C-19), 146.0 (C-5), 142.1 (C-16), 140.2 (C-4), 131.8 (C-17, 21), 131.1 (C-15), 128.9 (C-12), 124.3 (C-18, 20), 108.5 (C-3), 105.1 (C-6), 56.5, 56.2 (C-8, 10), 31.9 (C-11). IR ( $\text{cm}^{-1}$ ): 3100–2850 (–CH<sub>3</sub>, –CH), 1683 (C=O), 1342 (–CH<sub>3</sub>), 1259 1002 (C–O–C), 1631, 850 (–NO<sub>2</sub>). MS (ESI)  $m/z$  326.1 [M + H]<sup>+</sup>.



**(Z)-2-(3-hydroxybenzylidene)-5,6-dimethoxy-2,3-dihydro-1H-inden-1-one (TM-12)** Light yellow solid, m.p.: 101.1–102.4 °C, 85.4% yield, 98.4% HPLC purity. <sup>1</sup>H NMR (400 MHz, CDCl<sub>3</sub>):  $\delta$  = 7.54 (s, 1H, Ar–H), 7.35 (s, 1H, Ar–H), 7.32 (d, *J* = 8.0 Hz, 1H, Ar–H), 7.25 (d, *J* = 8.0 Hz, 1H, Ar–H), 7.14 (s, 1H, Ar–H), 6.98 (s, 1H, Ar–H), 6.87 (d, *J* = 8.4 Hz, 1H, Ar–H), 4.00 (s, 3H, OCH<sub>3</sub>), 3.97 (s, 2H, phCH<sub>2</sub>), 3.96 (s, 3H, OCH<sub>3</sub>). IR ( $\text{cm}^{-1}$ ): 3149 (–OH), 3000–2800 (–CH<sub>3</sub>, –CH), 1664 (C=O), 1311 (–CH<sub>3</sub>), 1255, 1004 (C–O–C). MS (ESI)  $m/z$  297.1 [M + H]<sup>+</sup>.

## Biology

### In vitro inhibition of monoamine oxidase

Recombinant human MAO-A and MAO-B (5 mg/mL) were obtained from Sigma–Aldrich, prealiquoted and stored at  $-70^{\circ}\text{C}$  according to the procedure referenced to preliminary work (Li et al. 2017).

### Effect of test compounds on self-induced $\text{A}\beta_{1-42}$ aggregation and disaggregation experiments by the ThT assay

In order to investigate the self-induced  $\text{A}\beta_{1-42}$  aggregation, a ThT-based fluorometric assay was performed (Sang et al. 2015). The details could reference our previous work (Sang et al. 2015).

### Transmission electron microscopy (TEM) assay

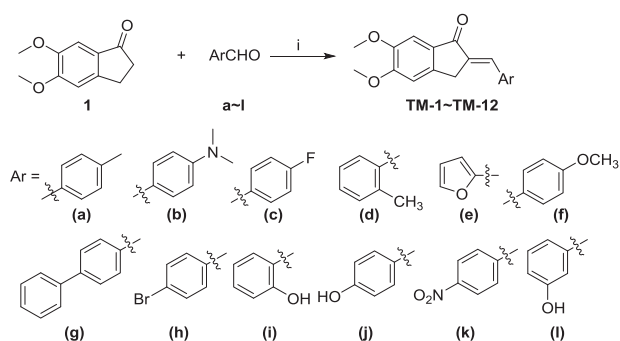
Briefly,  $\text{A}\beta_{1-42}$  was incubated within the presence and absence of compound **TM-11** at  $37^{\circ}\text{C}$  for 48 h. The final concentration of  $\text{A}\beta_{1-42}$  and test compound was  $25\ \mu\text{M}$ , respectively. Aliquots ( $50\ \mu\text{L}$ ) of each sample were placed on a carbon coated copper/rhodium grid for 2 min at room temperature. Each grid staining was performed with uranyl acetate (1%) for 2 min. the excess staining solution was discarded can the specimen was transferred for imaging with field emission transmission electron microscope (JEM-2100F) (Sang et al. 2019).

### Molecular modeling studies

The crystal structure of  $\text{A}\beta$  (PDB ID: 1BA4) were obtained from the Protein Data Bank after removing the original inhibitors and water molecules. The 3D Structure of **TM-11** was built and performed geometry optimization by molecular mechanics. Docking studies were performed using the AUTODOCK 4.2.6 program and each docked system was performed by 200 runs of the AUTODOCK search by the Lamarckian genetic algorithm. A cluster analysis was performed on the docking results using a root mean square tolerance of 1.0 and the lowest energy conformation of the highest populated cluster was selected for analysis. Graphic manipulations and visualizations were done by Autodock Tools or Discovery Studio 2.5 software (Sang et al. 2019).

### In vitro blood–brain barrier permeation assay

The blood–brain barrier penetration of compounds was evaluated using the parallel artificial membrane permeation assay (PAMPA) described by Di et al. 2003. The detailed



**Scheme 1** Synthesis of target compounds **TM-1** ~ **TM-12**. Reagents and conditions: (i) 50%KOH, EtOH, room temperature, 3 ~ 4 days

procedure could be found in our previous work (Sang et al. 2019).

## Results and discussion

### Chemistry

The synthetic route of the indanone–chalcone hybrid compounds was shown in Scheme 1. The target compounds were prepared by condensation of the starting material 5,6-dimethoxy-1-indanone (**1**) with the appropriate aldehydes (**a** ~ **l**) in ethanolic KOH solution. All new compounds were purified by recrystallization, and the analytical and spectroscopic data confirmed their structures, as detailed in the experimental section.

### Pharmacology

#### In vitro inhibition of monoamine oxidase

The inhibitory activity against MAO-A and MAO-B (recombinant human enzyme) was determined, and clorgyline, rasagiline, and iproniazid were also tested as reference compounds (Li et al. 2017). As shown in Table 1, all the indanone–chalcone hybrid compounds were effective in inhibiting MAO-B in the submicromolar range or lower, and all the target compounds showed weak MAO-A inhibitory activities. Therefore, all the synthesized compounds were efficient selective MAO-B inhibitors. The structure–activity relationship in Table 1 indicated that the substituent groups served as important role. The compounds (**TM-1**, **TM-2**, **TM-4**, and **TM-6**) possessing electron-donating group displayed higher inhibitory activities than compounds (**TM-3**, **TM-4**, **TM-5**, **TM-7**, **TM-9**, and **TM-12**) with electron-withdrawing group, except compounds **TM-8** and **TM-11** having good inhibitory potency with  $\text{IC}_{50}$  values of 0.059 and  $0.031\ \mu\text{M}$ . Meanwhile, the position of substituent

**Table 1** Inhibition and disaggregation of A $\beta$  aggregation and MAOs (MAO-A and MAO-B) inhibitory potency of target compounds and reference compounds

Comp.	Ar	Self-Induced A $\beta$ <sub>1-42</sub> aggregation IC <sub>50</sub> ( $\mu$ M) <sup>a,b</sup>		IC <sub>50</sub> ( $\mu$ M) <sup>b</sup>	
		Inhibition	Disaggregation	MAO-A <sup>c</sup>	MAO-B <sup>d</sup>
TM-1		31.6±0.66	n.t.	n.a.	0.062±0.0031
TM-2		46.7±0.78	n.t.	57.6±0.29	0.022±0.01
TM-3		16.3±0.01	n.t.	n.a.	0.32±0.31
TM-4		3.8±0.23	5.8±0.66	n.a.	0.41±0.20
TM-5		20.3±0.96	n.t.	19.7±0.43	0.62±0.36
TM-6		27.8±0.15	n.t.	n.a.	0.055±0.08
TM-7		22.7±0.58	n.t.	n.a.	0.86±0.04
TM-8		4.6±0.01	11.5±0.58	52.9±0.68	0.059±0.11
TM-9		18.8±0.23	n.t.	n.a.	1.3±0.33
TM-10		21.6±0.58	n.t.	63.6±0.87	0.26±0.77
TM-11		1.8±0.11	7.9±0.65	n.a.	0.031±0.14
TM-12		6.9±0.22	7.2±0.81	n.a.	1.8±0.13
Curcumin		26.7 ± 0.89	24.1± 0.57	n.t.	n.t.
clorgyline		n.t.	n.t.	0.0036±0.0001	5.68±0.02
rasagiline		n.t.	n.t.	2.59±0.01	0.088±0.003
iproniazid		n.t.	n.t.	3.18±0.03	1.78±0.01

Structures (Ar substituent group) are shown in Fig. 1. Compounds defined “no active” means percent inhibition less than 5.0% at a concentration of 1.0  $\mu$ M

n.t. not tested, n.a. no active

<sup>a</sup>Inhibition of A $\beta$  aggregation, the thioflavin T fluorescence method was used

<sup>b</sup>IC<sub>50</sub> values represent the concentration of inhibitor required to decrease enzyme activity by 50% and are the mean of three independent experiments, each performed in triplicate (SD = standard deviation)

<sup>c</sup>From recombinant human MAO-A

<sup>d</sup>From recombinant human MAO-B

group also affected the inhibitory activity, generally, the inhibitory activities were in order: 4-position > 2-position > 3-position, such as **TM-10** > **TM-9** > **TM-12**; **TM-1** > **TM-**

**4**. When the substituent group was furan group, the compound (**TM-5**) exhibited moderate inhibitory activity with IC<sub>50</sub> value of 0.62  $\mu$ M. Among these compounds,

compound **TM-2** was the best selective MAO-B inhibitor with  $IC_{50}$  value of 0.022  $\mu$ M.

### Effect of test compounds on self-induced $A\beta_{1-42}$ aggregation and disaggregation experiments by ThT assay

In order to assess the effects of the target compounds against self-induced  $A\beta_{1-42}$  aggregation, we carried out two individual studies: inhibition and disaggregation experiments of self-induced  $A\beta_{1-42}$  aggregation using the ThT fluorescence assay (Sang et al. 2015). Curcumin, a known active natural product for inhibition of self-induced  $A\beta$  aggregation, was used as reference compound. The results of inhibitory activity of  $A\beta_{1-42}$  aggregation were summarized in Table 1, almost all the target compounds exhibited more potent inhibition potency for self-mediated  $A\beta_{1-42}$  aggregation than curcumin ( $IC_{50} = 26.7 \mu$ M). According to the data, the properties of the substituent group had significant effects on  $A\beta$  aggregation inhibitory activities, generally, the electron-drawing group (**TM-3**, **TM-8**, and **TM-11**) in benzene ring indicated better inhibitory activities than that with electron-donating group (**TM-1**, **TM-2**, **TM-6**, **TM-7**, and **TM-10**). The position of substituent group of benzene ring also affected the inhibitory potency, when the substituent group were  $-OH$  and  $-CH_3$ , the inhibitory activities were in the order, 3-position > 2-position > 4-position, such as **TM-12** > **TM-9** > **TM-10**; **TM-6** > **TM-1**. Replacing the benzene ring substituent group of **TM-4** with furan group to obtain compound **TM-5**, dramatically, the inhibitory activity dropped down to  $IC_{50}$  value of 20.3  $\mu$ M. In short, compounds **TM-4**, **TM-8**, and **TM-11** showed the potent inhibitory activities with  $IC_{50}$  value of 3.8, 4.6, and 1.8  $\mu$ M.

Compounds **TM-4**, **TM-8**, **TM-11**, and **TM-12** were selected to test the disaggregation effects on self-induced  $A\beta_{1-42}$  aggregation using the ThT binding assay. According to the data in Table 1, compounds **TM-4**, **TM-8**, **TM-11**, and **TM-12** could significantly disaggregate  $A\beta$  fibrils with  $IC_{50}$  value of 5.8, 11.5, 7.9, and 7.2  $\mu$ M, respectively. From the above results, revealing that indanone–chalcone hybrid compounds could inhibit and disaggregate self-induced  $A\beta_{1-42}$  aggregation.

### Cytotoxicity

In order to evaluate the further biological activity of indanone–chalcone hybrid compounds, compounds **TM-3**, **TM-4**, **TM-5**, **TM-6**, **TM-8**, **TM-9**, and **TM-11**, with better inhibitory activity of self-induced  $A\beta_{1-42}$  aggregation, was selected to examine the cytotoxicity. SH-SY5Y cells were exposed to the test compounds at 1  $\mu$ M concentrations for 24 h, and the cell viabilities were tested by the 3-(4,5-dimethylthiazol-2-yl)-2,5-diphenyltetrazolium

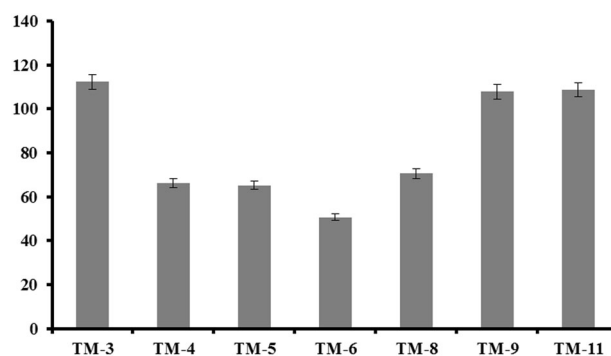


**Fig. 2** Effects of **TM-3**, **TM-4**, **TM-5**, **TM-6**, **TM-8**, **TM-9**, and **TM-11** on cell viability in SH-SY5Y cells. Data are mean values SEM of three independent experiments

(MTT) assays (Jiang et al. 2019). As shown in Fig. 2, **TM-4**, **TM-5**, **TM-6**, and **TM-8** induced a decrease of cell viability (66.1%, 65.2%, 50.6%, and 70.5%, respectively), while **TM-3**, **TM-9**, and **TM-11** did not show modified cell viability. The results showed that **TM-3**, **TM-9**, and **TM-11** had a wide therapeutic safety range.

### Transmission electron microscopy

According to the results of self-induced  $A\beta_{1-42}$  aggregation, compounds **TM-4**, **TM-8**, and **TM-11** showed similar inhibitory activities, but compound **TM-4** and **TM-8** displayed significant cytotoxicity. Therefore, compound **TM-11** should be encouraged to further studies.

To complement the ThT binding assay, the inhibition effect of **TM-4** on self-induced  $A\beta_{1-42}$  aggregation was also monitored by TEM (Fig. 3) (Sang et al. 2019). The results showed that the sample of  $A\beta_{1-42}$  alone had aggregated into amyloid fibrils after 24 h of incubation, while only small bulk aggregates were visible and no characteristic fibrils were observed in the sample of  $A\beta_{1-42}$  in the presence of compound **TM-11**. The TEM results were well consistent with the results of ThT measurements, which strongly proved that compound **TM-11** could inhibit  $A\beta_{1-42}$  fibrils formation.

### Molecular modeling studies

To further explore the binding modes of the active compound **TM-11** with  $A\beta_{1-42}$ , a molecular docking experiment was performed (Sang et al. 2019). The structure of  $A\beta$  used was downloaded from the Protein Data Bank (PDB: 1BA4). As shown in Fig. 4, compound **TM-11** was locked at the C-terminus hydrophobic area of  $A\beta$ . The oxygen atom of the methoxy group interacted with ASP1 through one intermolecular hydrogen bond, the  $-NO_2$  group hydroxyl could bind to LYS28 via two intermolecular hydrogen bond. In addition, compound **TM-11**

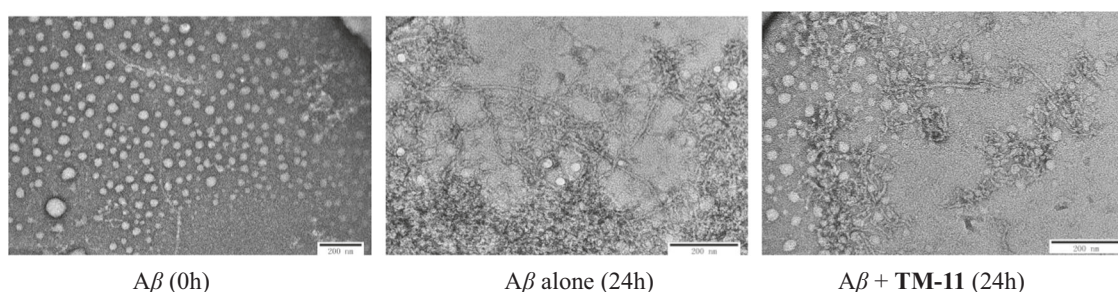


**Fig. 3** TEM images of  $A\beta_{1-42}$  (25  $\mu\text{M}$ ) in the presence and absence of 25  $\mu\text{M}$  compound **TM-11** after 24 h of aggregation

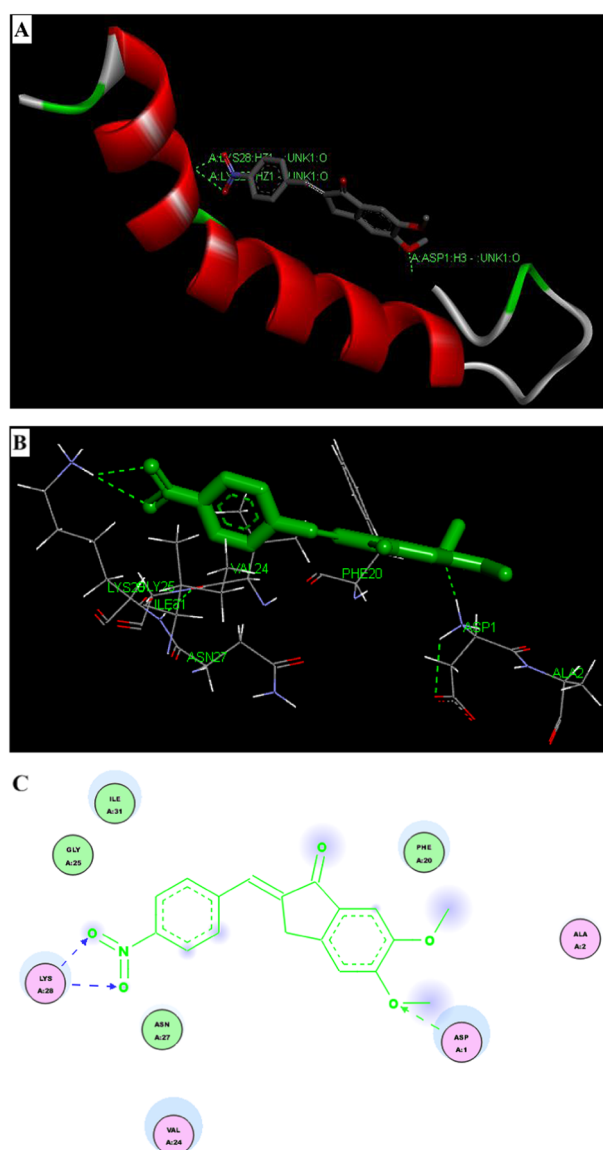


**Fig. 4** Docking studies of compound **TM-11** with  $A\beta_{1-42}$  (PDB ID: 1BA4). **a** Cartoon representations of compound **TM-11** interacting with  $A\beta_{1-42}$ . **b** Association of **TM-11** (green stick) and the C-terminus of obtained from docking calculations. **c** 2D schematic diagram of docking model of compound **TM-11** with  $A\beta_{1-42}$

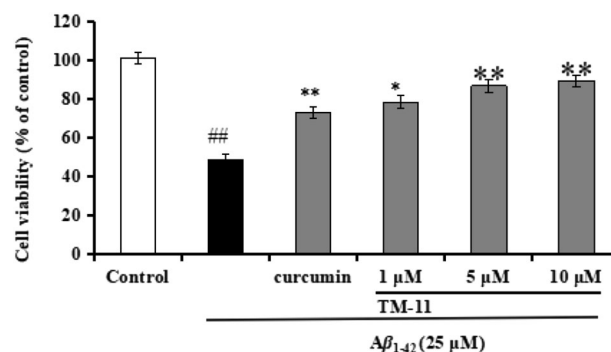


**Fig. 5** Neuroprotection against  $A\beta_{1-42}$ -induced toxicity, compound **TM-11** was tested for neuroprotective activity against  $A\beta$  toxicity in SH-SY5Y neuroblastoma cell cultures. Results are expressed as percent viability compared with untreated control. All data were expressed as mean  $\pm$  SD of three experiments. ## $p < 0.05$  vs control; \* $p < 0.05$ , \*\* $p < 0.01$  vs  $A\beta_{1-42}$  alone

**Table 2** Permeability  $P_e$  ( $\times 10^{-6}$  cm/s) in the PAMPA-BBB assay for 11 commercial drugs used in the experiment validation

Commercial drugs	Lit. (Di et al. 2003)	PBS:EtOH (70:30) <sup>a</sup>
Verapamil	16	16.90
Oxazepam	10	9.60
Diazepam	16	11.86
Clonidine	5.3	5.10
Imipramine	13	10.10
Testosterone	17	16.30
Caffeine	1.3	1.28
Enoxacin	0.9	0.47
Piroxicam	2.5	0.72
Norfloracin	0.1	0.42
Theophylline	0.12	0.10

<sup>a</sup>Data are the mean  $\pm$  SD of three independent experiments

formed the hydrophobic interactions with the residues ASP1, PHE20, LYS28, ASN27, and ILE31. These different interactions might be favorable for the binding of  $A\beta$  and compound **TM-11**.

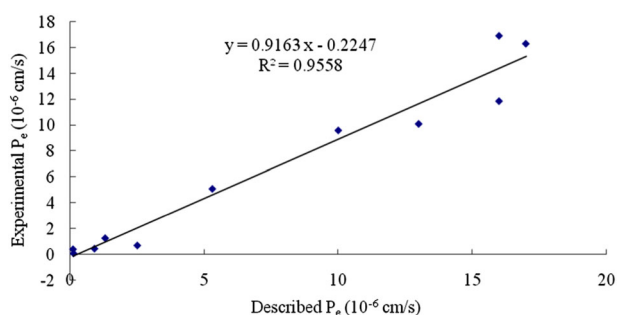


**Fig. 6** Linear correlation between experimental and reported permeability of commercial drugs using the PAMPA-BBB assay.  $P_e(\text{exp}) = 0.9163$ ,  $P_e(\text{bibl.}) - 0.2247$  ( $r^2 = 0.9558$ )

**Table 3** Ranges of permeability of PAMPA-BBB assays ( $P_e \times 10^{-6}$  cm/s)

Compounds of high BBB permeation (CNS+)	$P_e > 3.44$
Compounds of uncertain BBB permeation (CNS±)	$3.44 > P_e > 1.61$
Compounds of low BBB permeation (CNS-)	$P_e < 1.61$

**Table 4** Permeability  $P_e$  ( $\times 10^{-6}$  cm/s) in the PAMPA-BBB assay of the selected compound **TM-11** and the predictive penetration in the CNS

Compound <sup>a</sup>	$P_e$ ( $\times 10^{-6}$ cm/s) <sup>b</sup>	Prediction
<b>TM-11</b>	$12.36 \pm 0.89$	CNS+

<sup>a</sup>Compound **TM-11** was dissolved in DMSO at 5 mg/mL and diluted with PBS/EtOH (70:30). The final concentration of the compound was 100  $\mu\text{g/mL}$

<sup>b</sup>Values are expressed as the mean  $\pm$  SD of three independent experiments

**Table 5** Theoretical prediction of the ADME properties of compound **TM-11**

Comp. <sup>a</sup>	Log $P$	MW	TPSA ( $\text{\AA}^2$ )	n-ON	n-OH/NH	volume ( $\text{\AA}^3$ )
<b>TM-11</b>	3.32	325.32	81.36	6	0	282.24

MW Molecular weight, TPSA topological polar surface area, n-ON number of hydrogen acceptors, n-OH/NH number of hydrogen bond donors

<sup>a</sup>The data was determined with the Molinspiration calculation software

## Neuroprotective effect against $A\beta_{1-42}$ -induced neurotoxicity

$A\beta_{1-42}$ -induced apoptotic neuronal cell death was also an important factor in the pathology of AD. The representative compound **TM-11** was performed the further experiments against  $A\beta_{1-42}$ -induced neurodegeneration in the SH-SY5Y cells using MTT assay, curcumin was also evaluated as

control group (Jiang et al. 2019). As shown in Fig. 5, after 25  $\mu\text{M}$   $A\beta_{1-42}$  exposure for 48 h, cell viability obviously decreased to 48.5% ( $p < 0.01$ ) compared with untreated control. The cell viability increased to 72.7% after adding 5  $\mu\text{M}$  curcumin. When treatment with compound **TM-11** (1, 5, and 10  $\mu\text{M}$ ), the cell viability increased to 78.6, 86.8, and 89.5% in a dose-dependent manner, which showed better neuroprotective effect against  $A\beta_{1-42}$ -mediated neurotoxicity was than that with curcumin.

## In vitro blood–brain barrier permeation assay

The parallel artificial membrane permeation assay of the blood–brain barrier (PAMPA-BBB) was used to evaluate the possible blood–brain barrier (BBB) permeability of **TM-11** (Sang et al. 2019; Di et al. 2003). First, the assay was validated through comparing the permeability of 11 commercial drugs in Table 2. A good linear correlation,  $P_e(\text{exp}) = 0.9163P_e(\text{bibl.}) - 0.2247$  ( $r^2 = 0.9558$ ), was produced in Fig. 6. And then because of the known limit by Di et al., we considered that drug with permeability above  $3.44 \times 10^{-6}$  cm/s could cross BBB in vitro (Table 3). So, as shown in Table 4, **TM-11** could cross the BBB in vitro.

## Theoretical prediction of the ADME properties

To evaluate the druglike property of compound **TM-11**, the key parameters, such as log  $P$ , topological polar surface area (TPSA), the number of hydrogen-bond acceptors and hydrogen-bond donors were calculated using the Molinspiration property program (Matos et al. 2013). The results were shown in Table 5, compound **TM-11** complied with the Lipinski's rule of five, deserving the further study in vivo.

## Conclusion

In summary, a series of indanone–chalcone hybrid compounds were designed, synthesized, and evaluated as multifunctional agents for the treatment of AD. All the synthesized compounds showed remarkable MAO-B inhibitory activities and significant self-induced  $A\beta_{1-42}$  aggregation inhibition. Among these synthesized compounds, compound **TM-11** exhibited the best inhibitory potency of  $A\beta_{1-42}$  aggregation and good disaggregation activity with  $\text{IC}_{50}$  value of 1.8 and 7.9  $\mu\text{M}$ , both the TEM images and docking studies provided reasonable explain. Meanwhile, compound **TM-11** was a selective MAO-B inhibitor, as well as a neuroprotective agent against  $A\beta_{1-42}$ -induced toxicity. Moreover, **TM-11** could cross the BBB in vitro and accorded with the Lipinski's rule of five. Taken together, these results suggested that compound **TM-11** might be a potential multifunctional agent for the treatment of AD.

**Acknowledgements** This work was supported in part by the Foundation and Frontier Projects of Nanyang Science and Technology Bureau (2017JCQY020 and 2017 JCQY021). The Key Scientific Research Project of Colleges and Universities in Henan Province (20A350006). International Training of High-level Talents in Henan Province in 2019 (No. 17) (Henan Foreign Experts Bureau). The Special Project of Nanyang Normal University (SYKF2018081 and 2019QN001). Graduate Innovation Fund Project of Nanyang Normal University (No. 02).

## Compliance with ethical standards

**Conflict of interest** The authors declare that they have no conflict of interest.

**Publisher's note:** Springer Nature remains neutral with regard to jurisdictional claims in published maps and institutional affiliations.

## References

- Alzheimer's Disease International (2015) World Alzheimer Report 2015: the global impact of dementia. <https://www.alz.co.uk/research/world-report-2015>. Accessed Aug 2015
- Borroni E, Bohrmann B, Grueninger F, Prinssen E, Nave S, Loetscher H, Chinta SJ, Rajagopalan S, Rane A, Siddiqui A, Ellenbroek B, Messer J, Pähler A, Andersen JK, Wyler R, Cesura AM (2017) Sembragiline: a novel, selective monoamine oxidase type B inhibitor for the treatment of Alzheimer's disease. *J Pharmacol Exp Ther* 362(3):413–423
- Caliandro R, Pesaresi A, Cariati L, Procopio A, Oliverio M, Lamba D (2018) Kinetic and structural studies on the interactions of Torpedo californica acetylcholinesterase with two donepezil-like rigid analogues. *J Enzym Inhib Med Chem* 33(1):794–803
- Cavalli A, Bolognesi ML, Minarini A, Rosini M, Tumiatti V, Recanatini M, Melchiorre C (2008) Multi-target-directed ligands to combat neurodegenerative diseases. *J Med Chem* 51(3):347–372
- Costanzo P, Cariati L, Desiderio D, Sgammato R, Lamberti A, Arcone R, Salerno R, Nardi M, Masullo M, Oliverio M (2016) Design, synthesis, and evaluation of donepezil-like compounds as AChE and BACE-1 inhibitors. *ACS Med Chem Lett* 7(5):470–475
- de Freitas Silva M, Dias KST, Gontijo VS, Ortiz CJC, Vieira C (2018) Multi-target directed drugs: a modern approach for drug design towards Alzheimer's disease: an update. *Curr Med Chem* 25(29):3491–3525
- Di L, Kerns EH, Fan K, McConnell OJ, Carter GT (2003) High throughput artificial membrane permeability assay for blood–brain barrier. *Eur J Med Chem* 38(3):223–232
- Ferreira-Vieira TH, Guimaraes IM, Silva FR, Ribeiro FM (2016) Alzheimer's disease: targeting the cholinergic system. *Curr Neuropharmacol* 14(1):101–115
- Huang L, Lu C, Sun Y, Mao F, Luo Z, Su T, Jiang H, Shan W, Li X (2012) Multitarget-directed benzylideneindanone derivatives: anti- $\beta$ -amyloid ( $A\beta$ ) aggregation, antioxidant, metal chelation, and monoamine oxidase B (MAO-B) inhibition properties against Alzheimer's disease *J Med Chem* 55(19):8483–8492
- Jiang CS, Ge YX, Cheng ZQ, Wang YY, Tao HR, Zhu K, Zhang H (2019) Discovery of new selective butyrylcholinesterase (BChE) inhibitors with anti- $A\beta$  aggregation activity: structure-based virtual screening, hit optimization and biological evaluation. *Molecules* 24(14):pii: E2568
- Kumar B, Gupta VP, Kumar V (2017) A perspective on monoamine oxidase enzyme as drug target: challenges and opportunities. *Curr Drug Targets* 18(1):87–97
- Lane CA, Hardy J, Schott JM (2018) Alzheimer's disease. *Eur J Neurol* 25(1):59–70
- Li Y, Qiang X, Luo L, Li Y, Xiao G, Tan Z, Deng Y (2016) Synthesis and evaluation of 4-hydroxyl aurone derivatives as multi-functional agents for the treatment of Alzheimer's disease. *Bioorg Med Chem* 24(10):2342–2351
- Li Y, Qiang X, Luo L, Yang X, Xiao G, Zheng Y, Cao Z, Sang Z, Su F, Deng Y (2017) Multitarget drug design strategy against Alzheimer's disease: Homoisoflavonoid Mannich base derivatives serve as acetylcholinesterase and monoamine oxidase B dual inhibitors with multifunctional properties. *Bioorg Med Chem* 25(2):714–726
- Matos MJ, Vilar S, Gonzalez-Franco RM, Uriarte E, Santana L, Friedman C, Tatonetti NP, Viña D, Fontenla JA (2013) Novel (coumarin-3-yl)carbamates as selective MAO-B inhibitors: synthesis, in vitro and in vivo assays, theoretical evaluation of ADME properties and docking study. *Eur J Med Chem* 63:151–161
- Patil SA, Patil R, Patil SA (2017) Recent developments in biological activities of indanones. *Eur J Med Chem* 138:182–198
- Ricciarelli R, Fedele E (2017) The amyloid cascade hypothesis in Alzheimer's disease: it's time to change our mind. *Curr Neuropharmacol* 15(6):926–935
- Sang Z, Qiang X, Li Y, Yuan W, Liu Q, Shi Y, Ang W, Luo Y, Tan Z, Deng Y (2015) Design, synthesis and evaluation of scutellarein-O-alkylamines as multifunctional agents for the treatment of Alzheimer's disease. *Eur J Med Chem* 94:348–366
- Sang Z, Wang K, Han X, Cao M, Tan Z, Liu W (2019) Design, synthesis, and evaluation of novel ferulic acid derivatives as multi-target-directed ligands for the treatment of Alzheimer's disease. *ACS Chem Neurosci* 10(2):1008–1024
- Sensi SL, Granzotto A, Siotto M, Squitti R (2018) Copper and zinc dysregulation in Alzheimer's disease. *Trends Pharmacol Sci* 39(12):1049–1046
- Umar T, Hoda N (2017) Alzheimer's disease: a systemic review of substantial therapeutic targets and the leading multi-functional molecules. *Curr Top Med Chem* 17(31):3370–3389
- Zhuang C, Zhang W, Sheng C, Zhang W, Xing C, Miao Z (2017) Chalcone: a privileged structure in medicinal chemistry. *Chem Rev* 117(12):7762–7810